Deficits in axonal transport precede ALS symptoms in vivo

Lynsey G. Bilsland[a], Erik Sahai[b], Gavin Kelly[c], Matthew Golding[a], Linda Greensmith[d], and Giampietro Schiavo[a,1]

[a]Molecular NeuroPathobiology, [b]Tumour Cell Biology, and [c]Bioinformatics and Biostatistics Laboratories, Cancer Research UK London Research Institute, London WC2A 3LY, United Kingdom; and [d]Sobell Department of Motor Neuroscience and Movement Disorders, Institute of Neurology, University College London, London WC1N 3BG, United Kingdom

Edited* by Pietro De Camilli, Yale University and Howard Hughes Medical Institute, New Haven, CT, and approved October 5, 2010 (received for review May 18, 2010)

ALS is a fatal neurodegenerative disease characterized by selective motor neuron death resulting in muscle paralysis. Mutations in superoxide dismutase 1 (SOD1) are responsible for a subset of familial cases of ALS. Although evidence from transgenic mice expressing human mutant SOD1^{G93A} suggests that axonal transport defects may contribute to ALS pathogenesis, our understanding of how these relate to disease progression remains unclear. Using an in vivo assay that allows the characterization of axonal transport in single axons in the intact sciatic nerve, we have identified clear axonal transport deficits in presymptomatic mutant mice. An impairment of axonal retrograde transport may therefore represent one of the earliest axonal pathologies in SOD1^{G93A} mice, which worsens at an early symptomatic stage. A deficit in axonal transport may therefore be a key pathogenic event in ALS and an early disease indicator of motor neuron degeneration.

neurodegeneration | mitochondrial transport | p75^{NTR} neurotrophin receptor | motor neuron disease | sensory neuron

Axonal transport is fundamental for the maintenance of neuronal homeostasis. Neurons rely on anterograde transport for the movement of structural components and newly formed organelles along the axon and on retrograde transport for the transfer of organelles and ligands from synapses to the soma (1). Deficits in axonal transport have been proposed to contribute to the degeneration of motor and sensory neurons (2–4). For example, postnatal disruption of the microtubule-dependent motor KIF5A induces a reduction in slow anterograde transport, resulting in accumulation of neurofilaments in dorsal root ganglion (DRG) cell bodies, reduction in axonal caliber, and degeneration of sensory neurons (5). Similarly, the expression of KIF1Bβ mutants in mice induces slowing of the anterograde transport of synaptic vesicle precursors, resulting in a late-onset axonopathy (6). These pathological effects closely mimic those observed in individuals bearing mutations in the KIF5A and KIF1Bβ genes, which have been identified in families with hereditary spastic paraplegia (7) and Charcot-Marie-Tooth type 2A neuropathy (6), respectively. Other KIF genes and binding proteins have been recently associated with neurodegeneration (8, 9), and reduction in the levels of kinesin-associated protein 3 (KIFAP3) has been linked to increased survival in ALS patients (8), which may be due to changes in the axonal transport of choline acetyltransferase (ChAT) (10).

The relationship between axonal transport impairment and neurodegeneration is not unique to the kinesin motor family. Homozygous missense mutations in cytoplasmic dynein heavy chain (*Dync1h1*) reduce the rate of retrograde transport in motor neurons (MNs) and affect the survival of sensory neurons (11, 12). Targeted disruption of the dynein–dynactin complex by postnatal overexpression of the p50 dynactin subunit in mice induces late-onset MN degeneration (13), whereas mutations in the p150 dynactin subunit have been identified in families with a slowly progressing lower MN disease (14). Together, these observations indicate that defects in axonal transport are associated with neuronal degeneration.

Consistently, several lines of evidence suggest that deficits in both anterograde and retrograde transport contribute to ALS pathogenesis (3, 4, 10, 15–23). ALS patients and mice expressing mutant superoxide dismutase 1 (SOD1) display neurofilament accumulations, which may derive from defects in slow anterograde transport (19, 24, 25). Furthermore, alterations in fast axonal transport have been shown in embryonic SOD1^{G93A} MNs and inferred from postmortem human ALS axons (18, 25, 26). However, it is not clear how these deficits in axonal transport correlate with disease progression. In this study, we aimed to address this key question by developing an in vivo assay enabling the quantitative investigation of axonal retrograde transport in SOD1^{G93A} mice at different disease stages.

Results

Neurospecific Binding and Retrograde Transport of H_C in Vivo. A carboxyl-terminal fragment of tetanus toxin (H_C) binds with high affinity to the neuronal plasma membrane and enters endocytic carriers containing neurotrophins and their receptors in MNs and DRG neurons (27). H_C can therefore be used to monitor the axonal transport of these ligands and their effectors back to the soma in vivo. After injection into the tibialis anterior and gastrocnemius muscles, H_C accumulated at the neuromuscular junction (NMJ; *SI Appendix*, Fig. S1A) (28). Over time, the association of Alexa-Fluor555-H_C (H_C555) with the NMJ was reduced (*SI Appendix*, Fig. S1 *B* and *C*) owing to its uptake and sorting into the axonal shaft (*SI Appendix*, Fig. S1*D*). Transverse sections through the sciatic nerve at midthigh level 8 h after injection revealed H_C555 within axons (Fig. 1*A*), indicating that retrograde transport of this probe had occurred. These H_C555-positive axons were myelinated, and a large proportion (80% ± 5% SEM) stained positively for ChAT, an MN marker (Fig. 1*A*). H_C555 fluorescence was also visible in the perinuclear region of lumbar ventral horn MNs (Fig. 1*B*). Ipsilateral DRG somas were also positive for H_C555 (*SI Appendix*, Fig. S4*A*), consistent with previous data showing that H_C is also taken up by sensory neurons (29).

We were able to monitor the axonal transport of H_C555 in single axons in the intact sciatic nerve of WT mice (Movie S1). Transport of H_C555 occurred in the retrograde direction (Fig. 1*C*), with very rare anterograde or oscillatory movements (Fig. 1*D*). Moving organelles are shown in kymographs as diagonal traces, the slope of which is proportional to their speed and direction. Retrograde transport was not observed in the sciatic

Author contributions: L.B. and G.S. designed research; L.B. and M.G. performed research; E.S. and L.G. contributed new reagents/analytic tools; L.B., G.K., and G.S. analyzed data; and L.B. and G.S. wrote the paper.

The authors declare no conflict of interest.

*This Direct Submission article had a prearranged editor.

Freely available online through the PNAS open access option.

[1]To whom correspondence should be addressed. E-mail: giampietro.schiavo@cancer.org.uk.

This article contains supporting information online at www.pnas.org/lookup/suppl/doi:10.1073/pnas.1006869107/-/DCSupplemental.

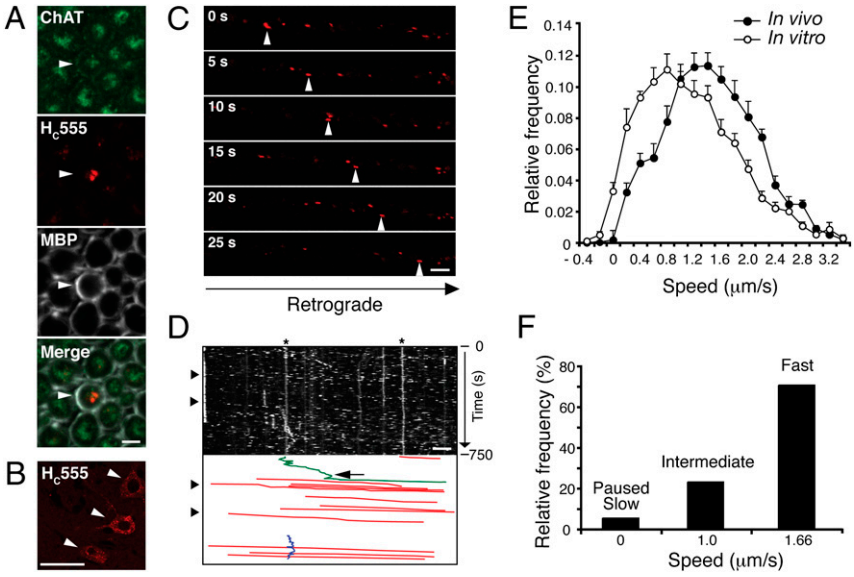

Fig. 1. Characterization of in vivo axonal retrograde transport in WT mice. (*A*) After i.m. injection, H_C555 was found within axons in transverse sections through the sciatic nerve, which costained for ChAT, an MN marker. Myelin sheaths were stained for myelin basic protein (MBP). (Scale bar, 5 μm.) (*B*) H_C555 was visible within the somas of lumbar MNs (arrowheads). (Scale bar, 50 μm.) (*C*) Images (movie stills) of axonal transport of H_C555 in the sciatic nerve were acquired by time-lapse confocal microscopy. (*D*) Corresponding kymograph. Retrograde carriers were moving to the right (arrowheads). Below the kymograph is a scheme reporting manually drawn lines tracing the movement of retrograde carriers (in red). Stationary carriers, labeled by asterisks, and carriers moving briefly in the anterograde direction (arrow; in green) or oscillating (in blue) were also present. (Scale bar, 5 μm.) (*E*) Comparison of the speed profiles of the H_C555 carriers in single axons revealed that retrograde transport was faster in vivo (filled circles; 258 carriers; 44 axons, $n = 5$ independent experiments) than in vitro (empty circles; 383 carriers; 32 axons, $n = 5$ independent cultures), with three defined speed components at 0–0.33 (slow), 1.0 (intermediate), and 1.66 μm/s (fast). The fastest speed component provided the major contribution to the overall speed profile of H_C555 carriers (*F*). Error bars represent SEM.

nerve of mice injected either with Texas Red–conjugated dextran or in untreated control animals. Kinetic analysis revealed that the average speed of H_C555 carriers in vivo (imaged in 44 axons from five independent experiments) was significantly faster than that observed in vitro in primary MNs (32 axons from five independent cultures), as shown by the right-hand shift of the curve (Fig. 1*E*; $P < 0.0001$), although within the range reported for fast axonal transport (1). Previous in vivo studies inferred average transport rates from the accumulation of radioactivity in the spinal cord at various time points after injection. In contrast, our assay allowed a real-time, quantitative assessment of the axonal retrograde transport of multiple cargoes in vivo (see below).

The speed distribution of retrograde carriers in cultured MNs was best described by the sum of speed components identified by Gaussian distributions centered at 0, 0.53, and 0.95 μm/s (details in *Materials and Methods*) (30). As expected by their speed distribution curve (Fig. 1*E*), axonal carriers visualized in the intact sciatic nerve displayed higher average velocities (0, 1.0, and 1.66 μm/s; Fig. 1*F*). This difference in speed may derive from the myelination of MN axons in sciatic nerves, which influences microtubule stability (31), or from differences between embryonic and adult MNs. The fastest speed component contributed ≈70% to the overall movement in vivo, with the intermediate and slowest components providing 25% and 5%, respectively (Fig. 1*F*). No age-related changes in the average speed of retrograde transport in adult WT mice were detected in this study (*SI Appendix*, Fig. S2; 38–125 d; 8–10 axons imaged per age group). However, because of the reported longer survival of female $SOD1^{G93A}$ mice (32), only female mice were used for further analyses.

Significant Deficits in Retrograde Transport in $SOD1^{G93A}$ Mice. We then assessed the appearance of retrograde transport defects in $SOD1^{G93A}$ mice, which were divided into four age groups representing different disease stages: presymptomatic (36 ± 0.95 d), early symptomatic (74 ± 1.7 d), symptomatic (95 ± 1.4 d), and late symptomatic (113 ± 3.5 d). Age-matched WT mice and mice overexpressing the WT human SOD1 gene ($SOD1^{WT}$) were used as controls. The different disease stages in $SOD1^{G93A}$ mice were characterized by quantifying the loss of sciatic MNs. Spinal cord sections from WT, early symptomatic, and late symptomatic $SOD1^{G93A}$ mice are shown in Fig. 2*A*. There was no significant difference in MN survival between WT and $SOD1^{WT}$ control mice (*SI Appendix*, Fig. S3*A*) or in $SOD1^{G93A}$ mice at a presymptomatic stage of disease. However, in early symptomatic $SOD1^{G93A}$ mice, which lacked overt disease signs (*SI Appendix*, Table S1), a significant number of MNs in the sciatic pool had already died (23% loss; Fig. 2*B*). With further disease progression, MN death increased to give a 39% and 56% loss in symptomatic and late symptomatic $SOD1^{G93A}$ mice, respectively (Fig. 2*B*).

Analysis of the retrograde transport of H_C555 in single axons in vivo revealed a significant slowing at each stage of disease in the $SOD1^{G93A}$ mice compared with both WT littermates (Fig. 2*C* and *SI Appendix*, Fig. S3 *D–F*; $P < 0.001$) and $SOD1^{WT}$ mice (*SI Appendix*, Fig. S3 *B* and *C*). A significant deficit in retrograde transport was observed in $SOD1^{G93A}$ mice even at 36 d (Fig. 2*C*; $P < 0.001$; 52 axons, $n = 6$ independent experiments). This deficit worsened with disease progression, as shown by the leftward shift of the speed curve at an early symptomatic stage (Fig. 2*C*; 39 axons, $n = 5$). The impairment in retrograde transport was still evident at both symptomatic (41 axons, $n = 6$) and late symptomatic stages (31 axons, $n = 4$), although to a lesser extent (Fig. 2*C*). Interestingly, H_C555 transport was faster in $SOD1^{WT}$ mice (30 axons, $n = 3$) than in WT littermates (*SI Appendix*, Fig. S3 *B* and *C*; $P < 0.001$), indicating that overexpression of $SOD1^{WT}$ significantly enhanced the transport kinetics of H_C555.

Deconvolution of the velocity curves shown in Fig. 2*C* highlighted a marked reduction in the fastest (1.66 μm/s) speed component in $SOD1^{G93A}$ mice at all disease stages compared with WT and $SOD1^{WT}$ mice, with a corresponding increase in the frequency of the intermediate speed carriers (1.0 μm/s; Fig. 2*D*). These changes occurred to a similar extent in presymptomatic, symptomatic, and late symptomatic $SOD1^{G93A}$ mice. However, early

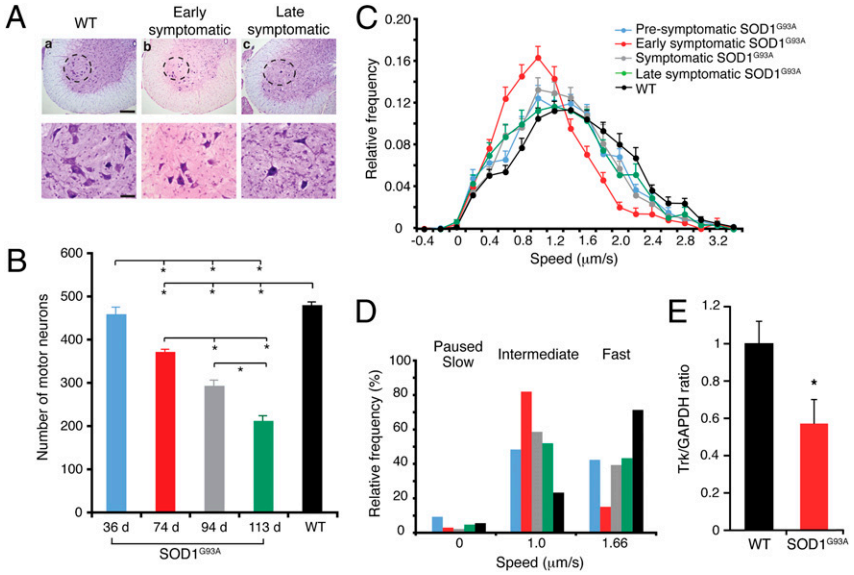

Fig. 2. Retrograde transport was reduced in SOD1^{G93A} mice. Disease stages were characterized by assessing MN loss. (*A*) Nissl-stained spinal cord sections, showing MNs in the sciatic motor pool (dashed areas, magnified below) of (*a*) WT, (*b*) early symptomatic, and (*c*) late symptomatic SOD1^{G93A} mice. [Scale bars, 200 μm (*Upper*) or 50 μm (*Lower*).] (*B*) No MN loss was detected at a presymptomatic stage, although death increased as disease progressed ($n = 6$). (*C*) Retrograde transport in single axons was assessed at four defined disease stages [presymptomatic (36 ± 0.95 d; 344 carriers; 52 axons, $n = 6$), early symptomatic (74 ± 1.7 d; 193 carriers; 39 axons, $n = 5$), symptomatic (95 ± 1.4 d; 250 carriers; 41 axons, $n = 6$), and late symptomatic (113 ± 3.5 d; 175 carriers; 31 axons, $n = 4$)] and in control WT mice (38-125 d; 258 carriers; 44 axons, $n = 5$). SOD1^{G93A} mice displayed a significant impairment in retrograde transport at a presymptomatic stage, which worsened by an early symptomatic stage. (*D*) Deconvolution analysis of the speed profiles. The slowing of transport in SOD1^{G93A} mice was due to a reduction in the fastest speed component and an increase in the intermediate component compared with WT. (*E*) Quantification of the TrkB antibody accumulated in the ligated sciatic nerve after i.m. injection also revealed a significant deficit in the axonal transport of this neurotrophin receptor in early symptomatic SOD1^{G93A} mice compared with WT. Bars represent the average TrkB signal normalized to GAPDH. Error bars represent SEM. *$P < 0.005$ or below ($n = 3$–6).

symptomatic mice showed the greatest decrease in the fastest speed component (Fig. 2*D*). The lessening in retrograde transport deficits in symptomatic and late symptomatic SOD1^{G93A} mice was not due to a failure of H_C555 uptake by affected MNs, because H_C555 accumulated at the NMJ (*SI Appendix*, Fig. S3*G*), was transported by motor axons (*SI Appendix*, Fig. S3*H*), and accumulated in lumbar MN somas (*SI Appendix*, Fig. S3*I*).

To confirm the results observed with H_C555 in vivo, we analyzed the transport of endogenous TrkB, the main neurotrophin receptor found in spinal cord MNs (33). We quantified the accumulation of a TrkB specific antibody at the site of sciatic nerve ligation 6 h after its injection in WT and SOD1^{G93A} mice at 75 d of age. Consistent with our previous results (Fig. 2*C*), a significant deficit in retrograde transport of TrkB was found in early symptomatic SOD1^{G93A} mice (Fig. 2*E*; $P < 0.005$).

Axonal Retrograde Transport Is Unaffected in SOD1^{G93A} Sensory Neurons. The sciatic nerve contains a mix of motor and sensory axons, and H_C555 was observed in DRG somas in addition to lumbar MNs (*SI Appendix*, Fig. S4*A*), raising the possibility that the deficits in axonal transport observed in SOD1^{G93A} mice were present in both motor and sensory neurons. After s.c. injection of H_C555 into the lateral hindpaw, we were able to specifically monitor retrograde transport in sensory axons of the sciatic nerve. Retrograde transport in these axons was slower than that observed after i.m. injection of H_C555 in WT mice (Fig. 3*A*) but did not significantly differ between WT (27 axons, $n = 3$) and early symptomatic SOD1^{G93A} mice (31 axons, $n = 3$). Similarly, retrograde transport in DRG neurons isolated from adult SOD1^{G93A} mice at varying disease stages was not significantly different from age-matched WT DRG neurons (*SI Appendix*, Fig. S4*B* and Movie S2; analysis of 10–29 axons from two or more independent experiments). Therefore, the deficit in axonal transport observed in the sciatic nerve in situ was not due to a deficit in sensory neurons but was likely to reflect a progressive impairment in the ability of MNs to sustain fast retrograde transport. Because the transport of H_C555 in sensory axons contributes to the overall speed distribution curve shown in Fig. 2*C*, the transport deficit in SOD1^{G93A} MNs may in fact have been underestimated.

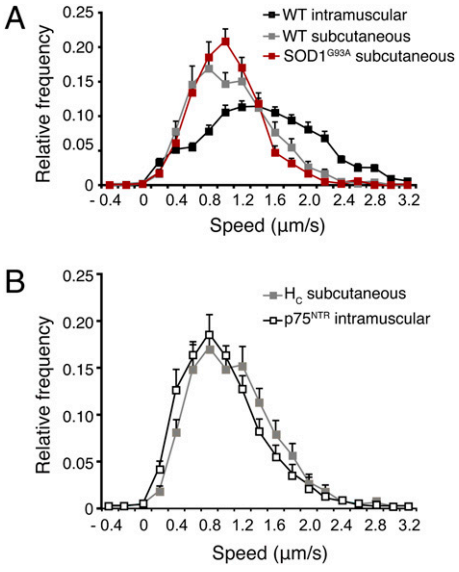

Fig. 3. In vivo analysis of axonal retrograde transport in sensory neurons. (*A*) s.c. injection allowed the selective endocytosis and retrograde transport of H_C555 in sensory neurons. H_C555 transport was significantly slower than that observed after i.m. injection. However, the transport kinetics in sensory neurons did not differ between WT (218 carriers; 27 axons, $n = 3$) and early symptomatic SOD1^{G93A} mice (215 carriers; 31 axons, $n = 3$). (*B*) Retrograde transport of AlexaFluor555-labeled anti-p75^{NTR} antibody injected i.m. was very similar to that of H_C555 after s.c. injection, thus implying that this p75^{NTR} antibody was specifically transported in sensory axons. Error bars represent SEM.

Interestingly, the kinetics of retrograde transport of an antibody specific for the extracellular domain of $p75^{NTR}$ upon i.m. injection were comparable to that seen after s.c. injection of H_C555 in WT mice (Fig. 3*B*; 24 axons, $n = 3$). The $p75^{NTR}$ receptor is not expressed in healthy MNs in adult mice (34), thus implying that this antibody was transported only in sensory axons. This $p75^{NTR}$ antibody therefore represents a useful tool to selectively assess defects in axonal trafficking in sensory neurons in vivo.

Alterations in Retrograde Transport in Legs at Odd Angles (*Loa*) Mice. To test the feasibility of our method on the analysis of axonal transport in another mouse model of neurodegeneration, we used the *Loa*/+ mouse, which carries a heterozygous missense mutation in cytoplasmic dynein heavy chain 1 ($Dync1h1^{Loa/+}$ or *Loa*/+) (11). This mutation causes a sensory deficit in mice, with a loss of more than 50% of lumbar proprioceptive neurons at 45 d of age (35). We therefore monitored the transport of H_C555 after i.m. injection in the sciatic nerve of *Loa*/+ mice at 75 d, an age equivalent to the early symptomatic stage in $SOD1^{G93A}$ mice. Two populations of carriers with distinct retrograde velocities were revealed (Fig. 4). In the first group (purple; 16 axons, $n = 2$), transport of H_C555 was not significantly different from that in WT mice (compare the purple curve in Fig. 4 and the black curve in Fig. 2*C*). However, a second group (orange; 14 axons, $n = 2$) showed transport rates even slower than those seen in $SOD1^{G93A}$ mice at the same age (compare the orange curve in Fig. 4 and the red curve in Fig. 2*C*) or observed for H_C555 in sensory neurons in WT mice (compare the orange curve in Fig. 4 and the gray curve in Fig. 3*A*). In light of the known sensory phenotype of *Loa*/+ mice, these slower axonal kinetics may represent transport of H_C555 in affected sensory neurons.

Onset of Axonal Transport Deficits Occurs in Presymptomatic $SOD1^{G93A}$ Mice. Consistent with recent work reporting reduced anterograde transport at 35–38 d in $SOD1^{G93A}$ mice (19), our study also identified significant deficits in axonal retrograde transport in this ALS model at a presymptomatic stage (Fig. 2*C*). Closer examination of our data revealed that the $SOD1^{G93A}$ mice at this stage could be categorized into two distinct subpopulations: the first in which the peak speed of retrograde transport overlapped with that of WT mice (30 axons, $n = 3$), and the second in which the peak speed was similar to that of early symptomatic animals (*SI Appendix*, Fig. S5*A*; 22 axons, $n = 3$). This presymptomatic stage (36 ± 0.95 d) might therefore represent the approximate age at which retrograde transport deficits in $SOD1^{G93A}$ mice first occur in vivo. To test this hypothesis, we assessed transport in younger $SOD1^{G93A}$ animals (25 ± 1.7 d), which lack any overt disease-related signs. In these mice, the rates of retrograde transport (*SI Appendix*, Fig. S5*A*) and speed distribution profiles (*SI Appendix*, Fig. S5*B*; 24 axons, $n = 3$) did not differ significantly from WT.

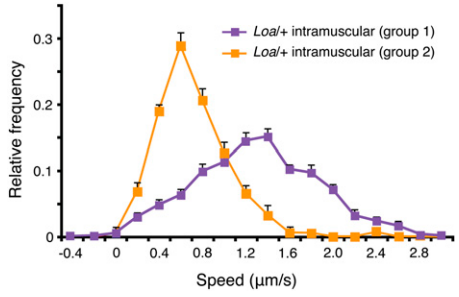

Fig. 4. Axonal transport deficits are evident in *Loa*/+ mice. Analysis of retrograde transport of H_C555 after i.m. injection in *Loa*/+ mice revealed two populations of carriers. The first population (in purple; 93 carriers; 16 axons, $n = 2$) had a speed profile almost indistinguishable from that of H_C555 upon i.m. injection in WT mice (Fig. 2*C*). The second population (in orange; 147 carriers; 14 axons, $n = 2$) had a speed profile slower than H_C555 transport in sensory axons after s.c. injection (Fig. 3*A*). Error bars represent SEM.

It has previously been reported that type IIb muscle fibers are denervated in $SOD1^{G93A}$ mice between 48 and 52 d of age (19, 36). To ensure that muscle denervation was not a contributing factor to the observed transport deficits at 36 d, we analyzed innervation of NMJs in the extensor digitorum longus and soleus muscles of WT and $SOD1^{G93A}$ mice. More than 500 endplates were counted for each muscle type, and no significant increase in denervation was found (*SI Appendix*, Fig. S6). This result suggests that muscle denervation is not a contributing factor to the observed deficit in retrograde transport at a presymptomatic stage.

In Vivo Transport of Mitochondria Is Altered in Presymptomatic $SOD1^{G93A}$ Mice. To investigate whether the deficits in axonal transport found in presymptomatic $SOD1^{G93A}$ mice were specific for these H_C555 carriers, we monitored mitochondrial dynamics in the sciatic nerve of $SOD1^{G93A}$thy1-mitoCFP-S mice. Neuronal mitochondria in the thy1-mitoCFP-S strain (also known as *MitoMouse*) are tagged with CFP (37). As expected, the lifespan of $SOD1^{G93A}$*MitoMouse* mutants did not differ from $SOD1^{G93A}$ mice, and H_C555 transport showed alterations similar to those observed in $SOD1^{G93A}$ animals, whereas transport in *MitoMouse* littermates was unaffected.

Analysis of mitochondria dynamics (Fig. 5*A*) revealed that there was a significant slowing in the rate of anterograde and retrograde transport of these organelles in presymptomatic $SOD1^{G93A}$*MitoMouse* mutants (Fig. 5*B*; $n = 4$ independent experiments) compared with *MitoMouse* controls ($n = 3$), although the peak speed in both cases was 0.4 μm/s (Fig. 5*B*). Neither the overall frequency of moving mitochondria in the sciatic nerve (Fig. 5*C*) nor the proportion of mitochondria transported in either anterograde or retrograde directions were statistically different between $SOD1^{G93A}$*MitoMouse* mutants and *MitoMouse* littermates at 36 d of age. However, pause analysis revealed that in $SOD1^{G93A}$*MitoMouse* mutants, both the proportion of mitochondria stopping *en route* (Fig. 5 *A* and *D*) and the average number of pauses in either direction (Fig. 5 *A* and *E*), were increased compared with *MitoMouse* littermates. As a control, the transport of mitochondria was analyzed in adult DRG neurons in vitro. No significant difference was observed between WT and $SOD1^{G93A}$ in either direction (*SI Appendix*, Fig. S7; analysis of 17–30 axons from three or more independent experiments). Altogether, our findings indicate that in $SOD1^{G93A}$ mice alterations in the axonal traffic of different classes of organelles occur specifically in MNs at a presymptomatic stage.

Discussion

The development of our in vivo assay has enabled the characterization of axonal transport of retrograde endosomes and mitochondria in single axons in the intact sciatic nerve and points to deficits in this process as one of the earliest pathological changes observed in $SOD1^{G93A}$ mice. Our results identify both the approximate age at which deficits in axonal retrograde transport first occur in $SOD1^{G93A}$ mice (36 d) and the worsening of this impairment during disease progression. In the $SOD1^{G93A}$ mouse model, the latter event may be related to the vulnerability of different MN pools in ALS pathogenesis. It has been suggested that there is a preferential susceptibility of fast MNs innervating type IIb (fast glycolytic) and IIa (fast oxidative) muscle fibers in $SOD1^{G93A}$ mice (19, 36, 38) and ALS patients (39). MNs are classified according to their firing pattern, which determines the phenotype of the muscle fibers they innervate (40). Fast, fatiguable (FF) and fast, resistant (FR) MNs innervate type IIb and IIa muscle fibers, respectively, and slow MNs innervate type I fibers. Synaptic vesicle stalling, indicative of impaired anterograde transport, has been observed in FF MNs at 35–38 d in $SOD1^{G93A}$

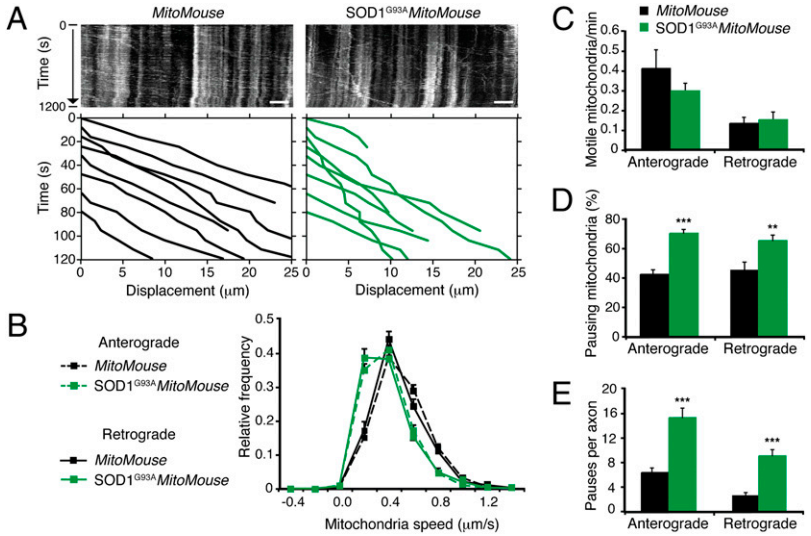

Fig. 5. Mitochondrial transport is affected in SOD1^{G93A} mice at a presymptomatic stage. Movement of CFP-tagged mitochondria was monitored in sciatic nerves of *MitoMouse* and SOD1^{G93A}*MitoMouse* mutants. (*A*) Examples of corresponding kymographs. Anterograde mitochondria were moving to the right. *Lower:* Representative traces of some of the tracked mitochondria. (Scale bar, 5 μm.) (*B*) SOD1^{G93A}*MitoMouse* axons displayed a significant impairment in both anterograde and retrograde transport of mitochondria (856 anterograde mitochondria in 161 axons and 380 retrograde mitochondria in 119 axons; $n = 4$) at a presymptomatic stage compared with *MitoMouse* littermates (670 anterograde mitochondria in 96 axons and 156 retrograde mitochondria in 61 axons; $n = 3$). (*C*) Kinetic analysis revealed no significant differences in the frequency of transported mitochondria in the sciatic nerve of SOD1^{G93A}*MitoMouse* and *MitoMouse* littermates. However, a higher percentage of mitochondria paused during transport in SOD1^{G93A}*MitoMouse* compared with *MitoMouse* controls (*D*), and more mitochondrial pauses per axon were also detected in SOD1^{G93A}*MitoMouse* than in controls (*E*), as also shown in *A*. Error bars represent SEM. $^{**}P < 0.01$, $^{***}P < 0.001$.

mice, with a reduction in synaptic vesicle markers by 38–46 d (*SI Appendix*, Table S1). Similarly, we saw a deficit in the axonal transport of both H_C555 and mitochondria in SOD1^{G93A} mice at 36 d, suggesting that defective axonal transport represents a disease marker in susceptible MNs at a presymptomatic stage.

Type IIb muscle fibers are denervated by 48–52 d in SOD1^{G93A} mice (19, 36), and although FR MNs partially reinnervate these muscles, this phenomenon is temporary, and by 80–90 d type IIa muscle fibers are also predominantly denervated (19). In contrast, slow MNs are more resistant to disease, and significant denervation of type I muscles does not occur until 120 d (36). Therefore, susceptible (and potentially already diseased) fast MNs might display reduced transport rates at an early symptomatic stage. This pool of neurons might therefore be responsible for the enhanced deficit in retrograde transport seen at the early symptomatic stage compared with the presymptomatic stage when no denervation or MN loss has occurred. In contrast, by the symptomatic stage, the majority of fast MNs have already been lost (19). Therefore, we hypothesized that the H_C555 signal observed at this symptomatic stage may represent axonal transport mainly in resistant MNs and a few, residual SOD1^{G93A}-susceptible neurons. The suggested contribution of different MN pools to the overall axonal transport at differing stages of disease in SOD1^{G93A} mice is summarized in *SI Appendix*, Table S1.

It is important to consider the contribution of sensory neurons when investigating axonal transport in the intact sciatic nerve. Our assay, which enabled us to selectively monitor transport in sensory axons after s.c. injection, showed that transport rates in sensory neurons were significantly slower than that seen after i.m. injection, which labeled both motor and sensory axons. Importantly, rates of axonal transport in sensory neurons did not differ between WT and SOD1^{G93A} mice, thus the transport defects seen in SOD1^{G93A} mice can be attributed to an impairment of retrograde transport only in MNs. We may therefore have underestimated this MN deficit due to the contribution of unaffected sensory axons.

Alterations in axonal transport in sensory neurons were evident in *Loa*/+ mice, in which a significant proportion of proprioceptive neurons are lost (35). In *Loa*/+ mice, sensory loss and transport deficits do not affect their lifespan (11, 12), whereas our study suggests that alterations in retrograde transport in SOD1^{G93A} mice may result in MN death and early mortality. This implies that deficits in retrograde transport in different types of neurons have different consequences for lifespan.

Mutant SOD1 interacts with the dynein–dynactin complex, forming aggregates in the spinal cord and sciatic nerve of SOD1^{G93A} mice (26, 41). This interaction is detectable at a presymptomatic stage (60 d) and increases with disease progression but does not occur with SOD1^{WT} (41). Thus, mutant SOD1 may sequester dynein within these aggregates, reducing the efficiency of dynein-mediated transport. In WT embryonic MNs, inhibition of dynein, which is critical for H_C trafficking, reduces the fastest speed component of retrograde transport (30). A similar effect is found in SOD1^{G93A} mice in vivo (Fig. 2*D*), suggesting that SOD1^{G93A} impairs dynein function. The binding of SOD1^{G93A} to mitochondria (25) may also reduce ATP production, thereby reducing its availability for dynein-mediated transport. This defect may be worsened by the accumulation of hyperdynamic microtubules in presymptomatic SOD1^{G93A} mice (42). This hypothesis is supported by our work showing deficits in the bidirectional transport of mitochondria in vivo in SOD1^{G93A} mice at a presymptomatic stage.

Surprisingly, retrograde transport in SOD1^{WT} mice was faster than in WT mice. The fastest speed component is by far the major contributor to the overall axonal retrograde transport in SOD1^{WT} mice. Although their molecular identities are presently unclear, the presence of multiple populations of carriers with different average speeds is likely to reflect the contribution of different motor complexes to the transport of axonal organelles. Therefore, the relative increase of the fastest speed component in SOD1^{WT} mice suggests that overexpression of SOD1^{WT} may enhance the efficiency of dynein-mediated transport or promote dynein recruitment to transport carriers. This may be linked to an increased antioxidant activity bestowed by SOD1^{WT} overexpression, whereas mutant SOD1 may not fulfill this role due to its mislocalisation and/or sequestration into aggregates (25).

A significant body of evidence now points towards a causal relationship between deficits in axonal transport and degeneration of susceptible MNs in ALS (2–4, 14, 22, 23). Deficits in axonal trans-

port have been observed before disease onset and may represent one of the first pathological signs of MN dysfunction. The impairment of fast retrograde transport in a particular neuron may therefore be a predictor of neurodegeneration. Thus, measurement of axonal transport in vivo may provide an early biomarker of disease progression and enable a timely diagnosis of MN impairment, when the disease may be more responsive to therapeutic intervention.

Materials and Methods

Details on animal handling, neuronal cultures, biochemical assays, immunohistochemistry, and statistical analysis are provided in *SI Appendix, SI Materials and Methods*. Purified H_C was prepared as previously described (30) and labeled with AlexaFluor555-maleimide according to the manufacturer's instructions, followed by dialysis against PBS to remove unbound dye. TrkB and $p75^{NTR}$ (27) antibodies were labeled with AlexaFluor555 using a monoclonal antibody labeling kit (Invitrogen).

In Vivo Retrograde Transport Assay. Mice were anesthetized with isoflurane (National Veterinary Services) and their tibialis anterior and gastrocnemius muscles exposed in one hindlimb. H_C555 (13 μg) and BDNF (50 ng), which has been previously shown to increase H_C internalization (43), were slowly injected either i.m. or s.c. in the foot pad using a microsyringe. The needle was left in place for 1 min to prevent leakage. Alternatively, an AlexaFluor555-labeled antibody directed against the extracellular domain of $p75^{NTR}$ was used. For control experiments, Texas Red–dextran was injected instead of H_C555. Six hours later, animals were reanesthetized and the sciatic nerve exposed. Mice were placed on a heated stage, covered with a heated blanket, and axonal transport was imaged in the intact sciatic nerve by time-lapse in vivo confocal microscopy. Images of axons were acquired every 5–8 s with an inverted Zeiss LSM 510 equipped with a plan apochromat 63× water immersion objective (N.A. 1.2), after the excitation of selected regions of interest with the 543-nm line of a helium–neon laser for H_C555 and AlexaFluor555-$p75^{NTR}$ antibody, and the 458-nm line of an argon laser for CFP-tagged mitochondria.

Tracking and Data Quantification. Tracking was performed as previously described (18, 30) using Motion Analysis software (Kinetic Imaging). Only moving carriers that could be tracked over at least four consecutive time points within a single axon were considered. Speed was determined by measuring the distance covered by the organelle between two consecutive frames. The speed distribution was obtained using a 0.2 μm/s binning interval and analyzed by applying a multiple Gaussian curve fit as previously described (18, 30) (KaleidaGraph v4.02; Synergy Software). Briefly, fitting with unimodal [$y = m_1 \times \exp(-(x - v_i)^2/{m_2}^2$; where v_i is the inferred average speed of the carriers] and bimodal Gaussian profiles failed to satisfactorily describe ($R^2 < 0.8$) the speed distribution curves of axonal carriers tracked in sciatic nerves of WT and $SOD1^{G93A}$ mice at different ages. Optimal fitting was obtained by using the sum of three Gaussian profiles centered at 0–0.33 (paused/slow), 1.0 (intermediate), and 1.66 μm/s (fast). Datasets considered for the analysis had an $R^2 \geq 0.98$. The contribution of each single speed component was determined by calculating the integral of the correspondent Gaussian curve and expressed as a percentage of the total.

Kymographs, which map the movement and direction of the axonal organelles, were generated by stacking the image time series of individual axons vertically over time.

ACKNOWLEDGMENTS. We thank Professor Ken Smith (Institute of Neurology, University College London) for generously donating the thy1-mitoCFP-S strain. This work was supported by the Motor Neurone Disease Association (L.B., L.G., and G.S.), the Jean Coubrough Charitable Trust (L.B., L.G., and G.S.), Cancer Research UK (L.B., E.S., G.K., M.G., and G.S.), the Vth Framework program of the the European Union (QLG3-CT-1999-00573), and the Brain Research Trust (L.G.).

1. Goldstein LS, Yang Z (2000) Microtubule-based transport systems in neurons: The roles of kinesins and dyneins. *Annu Rev Neurosci* 23:39–71.
2. Chevalier-Larsen E, Holzbaur EL (2006) Axonal transport and neurodegenerative disease. *Biochim Biophys Acta* 1762:1094–1108.
3. De Vos KJ, Grierson AJ, Ackerley S, Miller CC (2008) Role of axonal transport in neurodegenerative diseases. *Annu Rev Neurosci* 31:151–173.
4. Morfini GA, et al. (2009) Axonal transport defects in neurodegenerative diseases. *J Neurosci* 29:12776–12786.
5. Xia CH, et al. (2003) Abnormal neurofilament transport caused by targeted disruption of neuronal kinesin heavy chain KIF5A. *J Cell Biol* 161:55–66.
6. Zhao C, et al. (2001) Charcot-Marie-Tooth disease type 2A caused by mutation in a microtubule motor KIF1Bbeta. *Cell* 105:587–597.
7. Reid E, et al. (2002) A kinesin heavy chain (KIF5A) mutation in hereditary spastic paraplegia (SPG10). *Am J Hum Genet* 71:1189–1194.
8. Landers JE, et al. (2009) Reduced expression of the Kinesin-Associated Protein 3 (KIFAP3) gene increases survival in sporadic amyotrophic lateral sclerosis. *Proc Natl Acad Sci USA* 106:9004–9009.
9. Pasinelli P, Brown RHJ (2006) Molecular biology of amyotrophic lateral sclerosis: insights from genetics. *Nat Rev Neurosci* 7:710–723.
10. Tateno M, et al. (2009) Mutant SOD1 impairs axonal transport of choline acetyltransferase and acetylcholine release by sequestering KAP3. *Hum Mol Genet* 18:942–955.
11. Hafezparast M, et al. (2003) Mutations in dynein link motor neuron degeneration to defects in retrograde transport. *Science* 300:808–812.
12. Teuchert M, et al. (2006) A dynein mutation attenuates motor neuron degeneration in SOD1(G93A) mice. *Exp Neurol* 198:271–274.
13. LaMonte BH, et al. (2002) Disruption of dynein/dynactin inhibits axonal transport in motor neurons causing late-onset progressive degeneration. *Neuron* 34:715–727.
14. Dion PA, Daoud H, Rouleau GA (2009) Genetics of motor neuron disorders: New insights into pathogenic mechanisms. *Nat Rev Genet* 10:769–782.
15. Sasaki S, Iwata M (1996) Impairment of fast axonal transport in the proximal axons of anterior horn neurons in amyotrophic lateral sclerosis. *Neurology* 47:535–540.
16. Warita H, Itoyama Y, Abe K (1999) Selective impairment of fast anterograde axonal transport in the peripheral nerves of asymptomatic transgenic mice with a G93A mutant SOD1 gene. *Brain Res* 819:120–131.
17. Williamson TL, Cleveland DW (1999) Slowing of axonal transport is a very early event in the toxicity of ALS-linked SOD1 mutants to motor neurons. *Nat Neurosci* 2:50–56.
18. Kieran D, et al. (2005) A mutation in dynein rescues axonal transport defects and extends the life span of ALS mice. *J Cell Biol* 169:561–567.
19. Pun S, Santos AF, Saxena S, Xu L, Caroni P (2006) Selective vulnerability and pruning of phasic motoneuron axons in motoneuron disease alleviated by CNTF. *Nat Neurosci* 9:408–419.
20. De Vos KJ, et al. (2007) Familial amyotrophic lateral sclerosis-linked SOD1 mutants perturb fast axonal transport to reduce axonal mitochondria content. *Hum Mol Genet* 16:2720–2728.
21. Perlson E, et al. (2009) A switch in retrograde signaling from survival to stress in rapid-onset neurodegeneration. *J Neurosci* 29:9903–9917.
22. Lambrechts D, Robberecht W, Carmeliet P (2007) Heterogeneity in motoneuron disease. *Trends Neurosci* 30:536–544.
23. Ilieva HS, Polymenidou M, Cleveland DW (2009) Non-cell autonomous toxicity in neurodegenerative disorders: ALS and beyond. *J Cell Biol* 187:761–772.
24. Hirano A, et al. (1984) Fine structural study of neurofibrillary changes in a family with amyotrophic lateral sclerosis. *J Neuropathol Exp Neurol* 43:471–480.
25. Boillée S, Vande Velde C, Cleveland DW (2006) ALS: A disease of motor neurons and their nonneuronal neighbors. *Neuron* 52:39–59.
26. Ligon LA, et al. (2005) Mutant superoxide dismutase disrupts cytoplasmic dynein in motor neurons. *Neuroreport* 16:533–536.
27. Deinhardt K, et al. (2006) Rab5 and Rab7 control endocytic sorting along the axonal retrograde transport pathway. *Neuron* 52:293–305.
28. Roux S, et al. (2005) Internalization of a GFP-tetanus toxin C-terminal fragment fusion protein at mature mouse neuromuscular junctions. *Mol Cell Neurosci* 30:572–582.
29. Stöckel K, Schwab M, Thoenen H (1975) Comparison between the retrograde axonal transport of nerve growth factor and tetanus toxin in motor, sensory and adrenergic neurons. *Brain Res* 99:1–16.
30. Lalli G, Gschmeissner S, Schiavo G (2003) Myosin Va and microtubule-based motors are required for fast axonal retrograde transport of tetanus toxin in motor neurons. *J Cell Sci* 116:4639–4650.
31. Kirkpatrick LL, Brady ST (1994) Modulation of the axonal microtubule cytoskeleton by myelinating Schwann cells. *J Neurosci* 14:7440–7450.
32. Heiman-Patterson TD, et al. (2005) Background and gender effects on survival in the TgN(SOD1-G93A)1Gur mouse model of ALS. *J Neurol Sci* 236:1–7.
33. Yan Q, et al. (1993) Influences of neurotrophins on mammalian motoneurons *in vivo*. *J Neurobiol* 24:1555–1577.
34. Copray JC, et al. (2003) Expression of the low affinity neurotrophin receptor p75 in spinal motoneurons in a transgenic mouse model for amyotrophic lateral sclerosis. *Neuroscience* 116:685–694.
35. Ilieva HS, et al. (2008) Mutant dynein (Loa) triggers proprioceptive axon loss that extends survival only in the SOD1 ALS model with highest motor neuron death. *Proc Natl Acad Sci USA* 105:12599–12604.
36. Frey D, et al. (2000) Early and selective loss of neuromuscular synapse subtypes with low sprouting competence in motoneuron diseases. *J Neurosci* 20:2534–2542.
37. Misgeld T, Kerschensteiner M, Bareyre FM, Burgess RW, Lichtman JW (2007) Imaging axonal transport of mitochondria in vivo. *Nat Methods* 4:559–561.
38. Hegedus J, Putman CT, Gordon T (2007) Time course of preferential motor unit loss in the SOD1 ^{G93A} mouse model of amyotrophic lateral sclerosis. *Neurobiol Dis* 28:154–164.
39. Dengler R, et al. (1990) Amyotrophic lateral sclerosis: Macro-EMG and twitch forces of single motor units. *Muscle Nerve* 13:545–550.
40. Navarrete R, Vrbová G (1984) Differential effect of nerve injury at birth on the activity pattern of reinnervated slow and fast muscles of the rat. *J Physiol* 351:675–685.
41. Zhang F, et al. (2007) Interaction between familial amyotrophic lateral sclerosis (ALS)-linked SOD1 mutants and the dynein complex. *J Biol Chem* 282:16691–16699.
42. Fanara P, et al. (2007) Stabilization of hyperdynamic microtubules is neuroprotective in amyotrophic lateral sclerosis. *J Biol Chem* 282:23465–23472.
43. Roux S, et al. (2006) Brain-derived neurotrophic factor facilitates in vivo internalization of tetanus neurotoxin C-terminal fragment fusion proteins in mature mouse motor nerve terminals. *Eur J Neurosci* 24:1546–1554.